MEASUREMENTS AND SIMULATIONS OF ELECTRON-CLOUD-INDUCED TUNE SHIFTS AND EMITTANCE GROWTH AT CESRTA

S. Poprocki, J.A. Crittenden, D.L. Rubin, and S.T. Wang
CLASSE, Cornell University, Ithaca NY 14853

Abstract

Extensive measurements of electron-cloud-induced betatron tune shifts and emittance growth are presented for trains of positron and electron bunches at 2.1 and 5.3 GeV at various bunch populations. Measurements using a witness bunch with variable distance from the end of the train and variable bunch population inform the study of cloud decay and the pinch effect. Improved electron cloud buildup modeling using detailed information on photoelectron production properties obtained from recently developed simulations successfully describes the tune shift measurements after determining ring-wide secondary-yield properties of the vacuum chamber by fitting the model to data. Space-charge electric field maps of the cloud from the validated model are then incorporated into a multiparticle tracking simulation of the beam through the lattice with electron cloud elements in the dipoles and field-free regions. The simulations predict emittance growth in agreement with the measurements.

INTRODUCTION

The buildup of low-energy electrons in the vacuum chamber along a train of positron bunches (See Fig. 1) can cause tune shifts, beam instabilities, and incoherent emittance growth. These electron cloud (EC) effects have been observed in many positron and proton storage rings [1], and can be a limiting factor in accelerator performance. Electron cloud effects have been observed and studied at the Cornell Electron-Positron Storage Ring (CESR) Test Accelerator (CESRTA) since 2008. Figure 2 shows a schematic of the CESR synchrotron and storage ring. A comprehensive summary of these studies which include mitigation methods can be found in [2].

First, we present measurements of vertical and horizontal emittance growth along a train of positron bunches followed by a witness bunch, with comparison to corresponding measurements using electron bunches, at 2.1 GeV. The bunch current and distance of the witness bunch beyond the end of the train are varied to study the pinch effect and the decay of the cloud, respectively.

Next, methods of betatron tune shift measurement are discussed and compared. A comprehensive set of measurements along trains of positron bunches at 2.1 GeV and 5.3 GeV are shown.

Lastly, we describe the full procedure of electron cloud simulation starting with the generation of photons from synchrotron radiation, tracking of the photons in a 3D model of the vacuum chamber including reflections, absorption of the photons and their production of primary electrons, the buildup of cloud along a train of bunches, calculation of betatron tunes, and ultimately particle tracking of a beam through the CESR lattice with electron cloud elements in dipoles and field-free regions. Although electron cloud buildup models have been successful in simulating tune shifts [3, 4] and vertical emittance growth [5] in general agreement with measurements, their predictive power has been limited by the large number of free parameters. Furthermore, no single set of parameters could reproduce in simulation, measurements of horizontal and vertical tune shifts over a wide range of bunch currents and beam energies.

In an effort to improve the predictive power of the model for tune shifts and emittance growth, we have recently employed the Synrad3D [6] and Geant4 [7] codes to calculate azimuthal distributions of absorbed photons, quantum efficiencies, and photoelectron energy distributions around the vacuum chamber throughout the circumference of the CESR ring [8]. Secondary yield parameters are fit to the large dataset of betatron tune shift measurements collected at CESR. The validated model is then used in improved simulations of vertical emittance growth, achieving good agreement with the measurements.

EMITTANCE GROWTH MEASUREMENTS

Bunch-by-bunch, turn-by-turn vertical beam size measurements were taken with an X-ray-based beam size monitor [9]. Additionally, single-shot bunch-by-bunch horizontal beam size measurements were collected using a gated camera [10]. Bunch-by-bunch feedback is used on all bunches for size measurements, to minimize centroid motion and associated coherent emittance growth. All measurements of emittance growth are done at 2.1 GeV and 14 ns bunch spacing. Figure 3 shows vertical emittance growth along a 30-bunch train of positron bunches for values of the bunch current ranging between 0.36 and 0.72 mA/b. No vertical beam size blowup is observed for bunch currents below 0.5 mA/b, and a current of 0.7 mA/b produced a blowup of a factor of four of the initial bunch size. For this reason, we focus on measurements (and simulations) at two currents: 0.4 mA (0.64×10^{10} bunch population) which is below the vertical blowup threshold, and 0.7 mA (1.12×10^{10}) which produces significant blowup. Measurements at these currents were repeated for trains of electrons, and the results are shown in Fig. 4 for both the vertical and horizontal bunch sizes. Emittance growth along the bunch train is observed only for positron bunches with currents exceeding the threshold current, and is seen in both the vertical and horizontal planes.

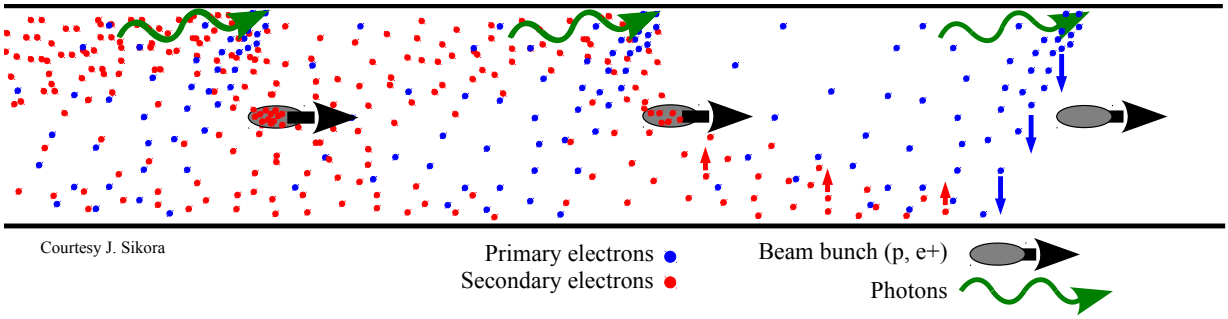

Figure 1: Depiction of electron cloud build-up in the vacuum chamber along a train of positively charged bunches moving left to right, at a specific point in time. Photons emitted via synchrotron radiation (caused by an upstream bending magnet) strike the outside wall of the vacuum chamber and produce electrons via the photoelectric effect or atomic de-excitation processes. These primary electrons (blue dots) may hit the vacuum chamber wall and produce secondary electrons (red dots). Electrons are accelerated by the passage of trailing bunches and produce more secondary electrons. The attraction of electrons into the bunch, known as the pinch effect, is also depicted.

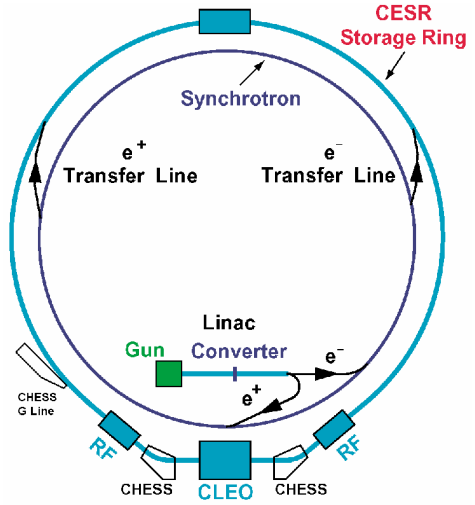

Figure 2: Schematic diagram of the CESR linac, synchrotron, and storage ring. Positrons circulate in the clockwise direction (top-down) and electrons anti-clockwise. The storage ring circumference is 768 m.

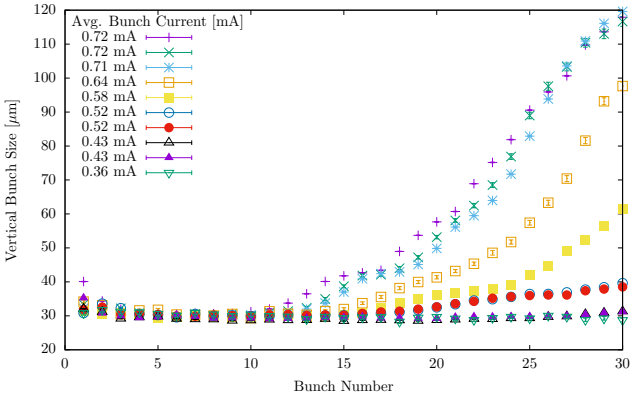

Figure 3: Vertical emittance growth along a 30 bunch train of positrons at 2.1 GeV, for a range of bunch currents. A bunch current of 1 mA corresponds to a bunch population of 1.6×10^{10} particles. Vertical blowup is observed for bunch currents above 0.5 mA/b.

Electron bunches did not show emittance growth at either current, which suggests the mechanism for the observed emittance growth is due to the attraction of the positron bunches and cloud electrons.

Measurements of vertical bunch size for a witness bunch are shown in Fig. 5. A single positron witness bunch follows a 30 bunch train of positrons at 0.7 mA/b. The witness bunch is initially injected into bunch position 60 at a current of 0.25 mA. Note that the ring can fit 183 bunches at a bunch spacing of 14 ns. The witness bunch size is measured, and its current increased to 0.5 mA. This process is repeated until the witness bunch has been measured at 1.0 mA, at which time it is ejected by disabling its feedback and giving it a kick via the feedback system. The witness bunch is then injected closer to the end of the train and measurements repeated until the witness bunch reaches the end of the train. By way of this back to front procedure, measurements of emittance growth are insensitive to residual charge that may be left in buckets where the charge is not completely ejected.

Vertical emittance growth is seen to depend on both the distance of the witness bunch to the train, which determines the cloud density seen by the witness bunch, and the bunch current of the witness bunch, which determines the strength of the pinch effect (*i.e.* cloud electrons being pulled into the positively charged bunch).

TUNE SHIFT MEASUREMENTS

Tune shifts have been measured in a number of ways at CESRTA. Coherently kicking the bunch train once ("pinging") and measuring the bunch-by-bunch, turn-by-turn bunch positions yields a fast measurement of the tune shift after peak-fitting the FFTs [2, 11]. However, multiple peaks from coupled-bunch motion contaminate the signal. In addition, only vertical tune shift measurements using vertical pinger kicks are reliable with this method. The development of a vertical band of electron cloud density in dipole mag-

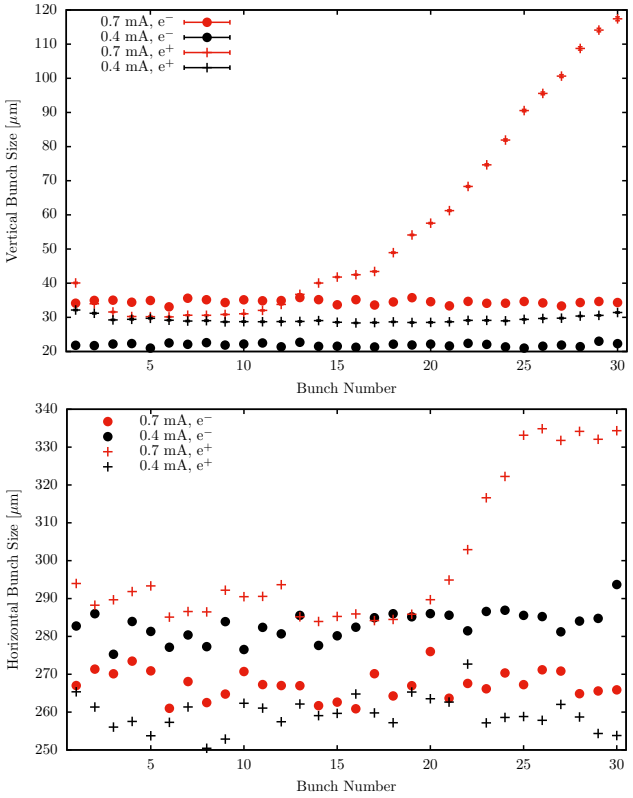

Figure 4: Vertical (top) and horizontal (bottom) bunch size along a 30 bunch train of positrons (+) and electrons (•) at 2.1 GeV for two different bunch currents: 0.4 mA/b (0.64×10^{10} particles) (black) and 0.7 mA/b (1.12×10^{10} particles) (red).

nets (see next section), *i.e.* a strong horizontal asymmetry on the scale of the beam size, is an important contribution to the tune shifts. A horizontal ping kick moves the bunch train coherently, and thus the cloud as well, so the measured horizontal tune shifts are suppressed by this measurement technique, since the test bunch receives no coherent kick from a cloud symmetric about its position. Better results are obtained by enabling bunch-by-bunch feedback on the train, disabling it one bunch at a time and measuring the tune of that bunch. The self-excitation (no external kick applied) is enough to get a signal, but the precision can be improved by kicking the single bunch with a gated stripline kicker. In the latest measurements we improve on this technique further by utilizing a digital tune tracker which excites the bunch via a transverse kicker in a phase-locked loop with a beam position monitor.

Tune shifts using the pinging method for 20 bunch trains of positrons at 5.3 GeV at various bunch currents are shown in Fig. 6. Large bunch-to-bunch fluctuations as well as overlap of data are seen compared to the same measurements obtained using the digital tune tracker, shown in Fig. 7, wherein the vertical tune shift increases monotonically with bunch current. However, the horizontal tune shift shows a remarkable behavior whereby the tune shift along the train decreases

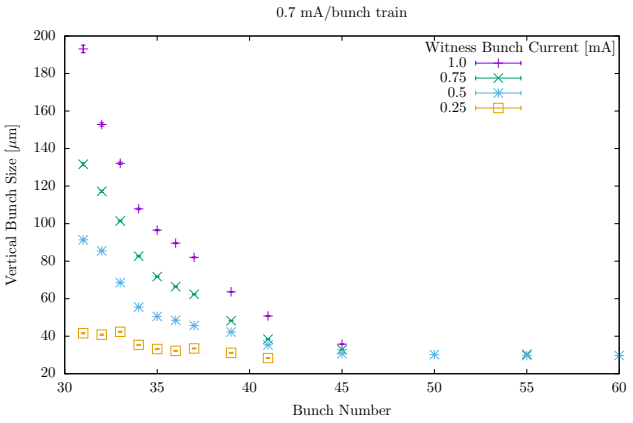

Figure 5: Vertical bunch size of a positron witness bunch at four different bunch currents (0.25, 0.5, 0.75, and 1.0 mA) trailing a 30 bunch train of 0.7 mA/b positrons at 2.1 GeV. Note that a single witness bunch is present for each measurement. The witness bunch current, which controls the strength of the pinch effect, is seen to have a large effect on the vertical bunch size.

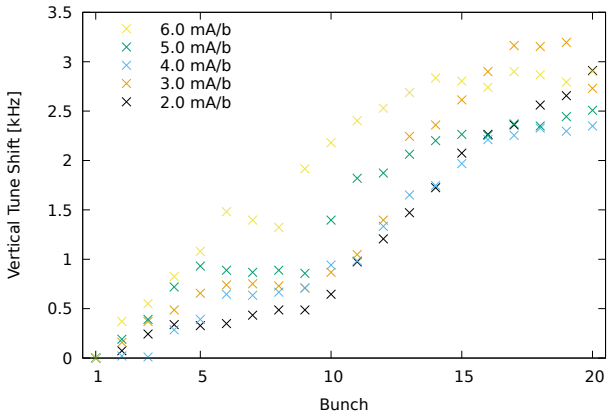

Figure 6: Vertical betatron tune shifts in kHz (to be compared to the revolution frequency of 390 kHz), measured using the "pinging" method, along a 20-bunch train of positrons at 5.3 GeV for values of the bunch current ranging from 2 to 6 mA/b ($3.2–9.6 \times 10^{10}$ bunch populations).

with later bunches and higher currents. Our modeling shows this effect to be due to the "cloud splitting" behavior in dipoles where the vertical stripe of cloud splits into two stripes due to cloud electron energies surpassing the peak energy of the secondary emission yield (SEY) curve due to the greater kicks from higher bunch populations.

Tune shift measurements taken with the digital tune tracker for positrons at 2.1 GeV are shown in Fig. 8. The horizontal tune shift shows a significant sensitivity to the bunch current, wherein the total horizontal tune shift increases by more than a factor of 5 when increasing the bunch current from 0.4 to 0.7 mA/b.

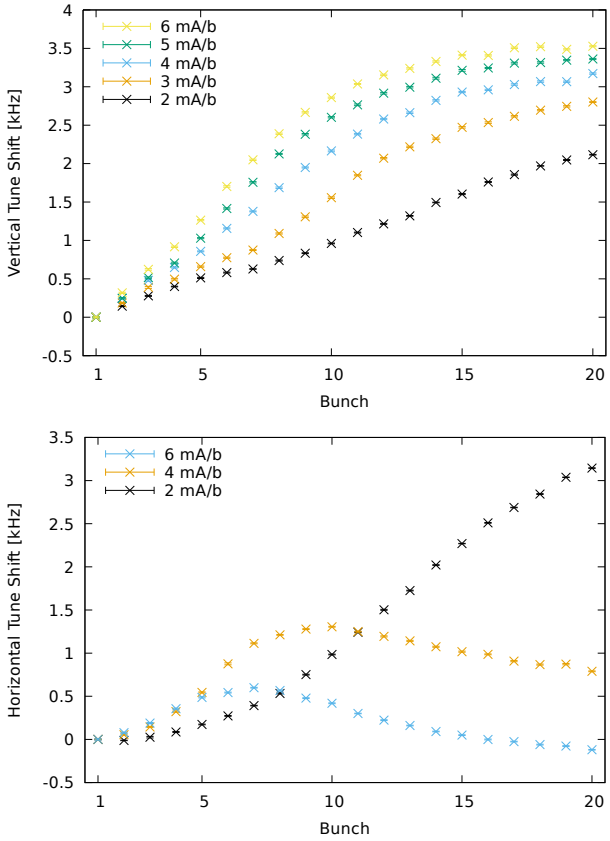

Figure 7: Vertical (top) and horizontal (bottom) tune shifts in kHz (to be compared to the revolution frequency of 390 kHz), measured using the digital tune tracker, for a 20 bunch train of positrons with values for the bunch current ranging between 2 and 6 mA/b (3.2–9.6×10^{10} bunch populations) at 5.3 GeV. Data were taken in each plane separately, and only at 2, 4, and 6 mA/b in the horizontal plane. These measurements are more reliable than those obtained via the pinging method (Fig. 6).

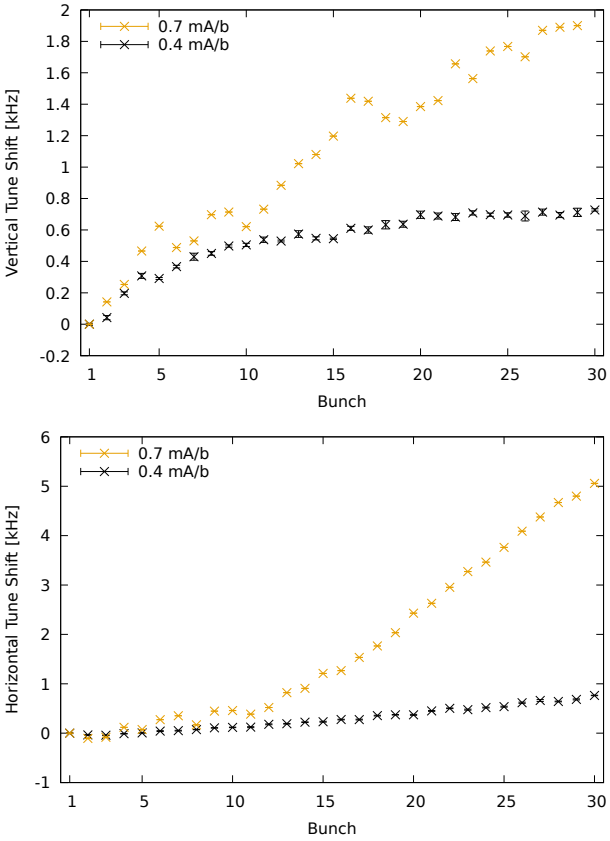

Figure 8: Vertical (top) and horizontal (bottom) tune shifts in kHz (to be compared to the revolution frequency of 390 kHz), measured using the digital tune tracker, for a 30 bunch train of positrons at 0.4 and 0.7 mA/b (0.64×10^{10} and 1.12×10^{10} bunch populations) at 2.1 GeV. The fluctuations in the vertical tune shift measurements at 0.7 mA/b were avoided for the other measurements by using an improved averaging method.

SIMULATIONS

The simulation pipeline involves running four different codes which feed into each other. The first step is simulation of photon generation from synchrotron radiation, and the subsequent tracking of photons including reflections in a detailed 3D vacuum chamber model of the entire CESR ring. This simulation results in information on individual photons absorbed in the vacuum chamber wall. The interaction of those absorbed photons with the vacuum chamber wall is then modeled in a Geant4-based simulation of electron production via the photoelectric and Auger effects. Quantum efficiencies and photoelectron energy distributions are obtained differentially in absorption site location both tranversely and around the ring. These first two steps are described in detail in Ref. [8]. The resulting data is then input into the electron cloud buildup simulation to model the generation of primary electrons. Time-dependent space-charge electric field maps from the cloud are obtained and used to calculate tune shifts. Finally, the field maps are incorporated into a particle tracking simulation of the beam through the full CESR lattice with EC elements overlaid on each dipole and field-free element. This allows for simulation of the equilibrium beam sizes.

These four simulation steps, along with a method of SEY parameter determination, will be discussed in more detail below.

Tracking photons from synchrotron radiation

This simulation is done using the Synrad3D code developed at Cornell University. Individual photons are generated according to a synchrotron radiation analysis of the lattice using the Bmad library [12]. A three dimensional description of the vacuum chamber geometry as well as the vacuum chamber materials is also supplied. A 5 nm layer of carbon monoxide on aluminum was found to be most consistent with photon reflectivity measurements of our vacuum chamber [6]. Photon scattering off the vacuum chamber walls is simulated using both smooth surface specular re-

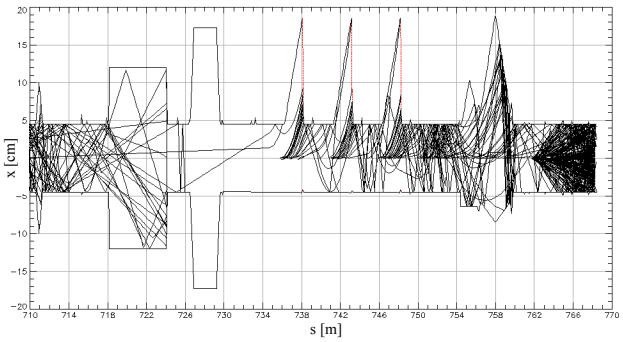

Figure 9: Top down view (x vs. s) for a portion of the CESR ring, showing photon tracks (black lines). The red vertical lines represent X-ray beam line exit ports, and any photon hitting those surfaces are terminated and not included in the calculation of photon absorption rates.

flections, according to the X-ray absorption data from the LBNL database [13] for the local material definition, as well as diffuse scattering via an analytic model for a finite surface roughness.

Figure 9 shows a plan view of photon trajectories in a region of the CESR ring which includes X-ray beamline exit windows, where incident photons are not included in the tally of electron-producing photon strikes.

Examples of the type of output data obtained from these simulations is shown in Fig. 10. In particular, for the subsequent simulation step, we obtain for each absorbed photon its azimuthal angle, energy, and grazing angle with the vacuum chamber wall.

Photoelectron production

The simulation of electron production from the photoelectric and Auger effects was performed using the Geant4 simulation toolkit [7, 14]. The absorbed photon data is split into 720 azimuthal bins, and for each bin, individual photons with the given energy and grazing angle are simulated to strike the vacuum chamber, which is modeled as a 5 nm layer of CO on aluminum. The number of electrons produced which come back into the vacuum (see Fig. 11), as well as their energies, are stored. The result is quantum efficiencies in each of the 720 azimuthal bins, as well as electron energy distributions in three azimuthal regions. Since the quantum efficiency depends on both photon energy and grazing angle, and these vary greatly azimuthally for the absorbed photons, so too does the quantum efficiency. Taking this into account in the EC buildup simulations, rather than assuming a single number for quantum efficiency, is a crucial improvement to the model and its predictive ability. Similarly, using the electron energy distributions from these simulations reduces the number of free parameters and assumptions. The simulations are done separately for dipole and field-free regions. See Ref. [8] for details.

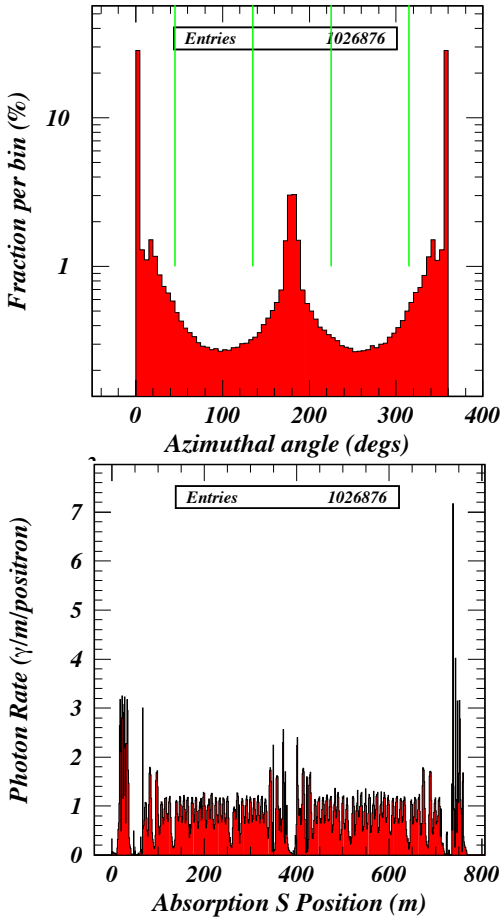

Figure 10: A sample of the information output by the Synrad3D simulation of photons from synchrotron radiation. Top: transverse azimuthal distribution of absorbed photons, where the angle origin is in the horizontal midplane on the outer wall of the beampipe. Note the log scale. Photons typically are absorbed on the outer wall with no prior reflections, or the inner wall after reflecting once, or, more rarely, absorbed on the top/bottom of the vacuum chamber after multiple reflections. Bottom: Photon absorption rate vs. s position around the ring.

Electron cloud buildup

The EC buildup simulation is based on extensions [11] to the ECLOUD [15] code. The beam size used in these simulations for the 2.1 GeV beam is ring-averaged and weighted by the element lengths for either the 800 Gauss dipole magnets or the field-free drift regions, and roughly 730 (830) microns horizontally for dipoles (drifts) and 20 microns vertically. The large ring-averaged horizontal size is dominated by dispersion effects. In these simulations we clearly see the pinch effect of the beam attracting the EC (Fig. 12). Electric field maps on a 15×15 grid of $\pm 5\sigma$ of the transverse beam size are obtained for 11 time slices as the bunch passes through the cloud. The time between slices is 20 ps. Figure 13 shows these field maps in a dipole for bunch number 30 in the 0.7 mA/b train during the central time slice. Since only a

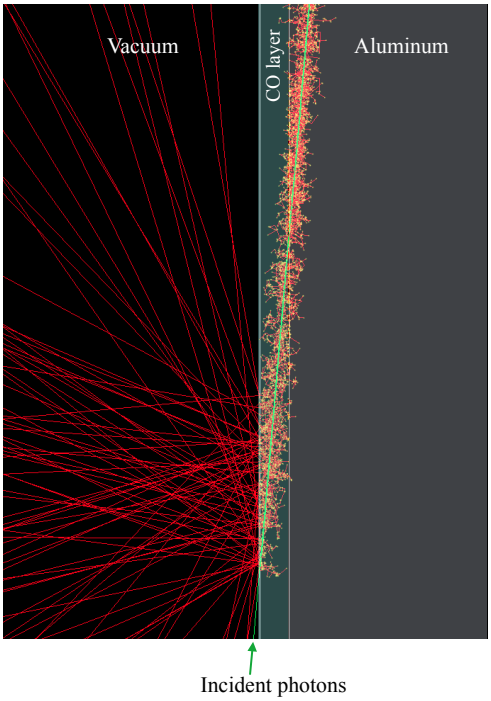

Figure 11: Tracks from incident 300 eV photons (green) and subsequently generated electrons (red) from Geant4. The outgoing angular distribution of electrons is normal to the surface on average.

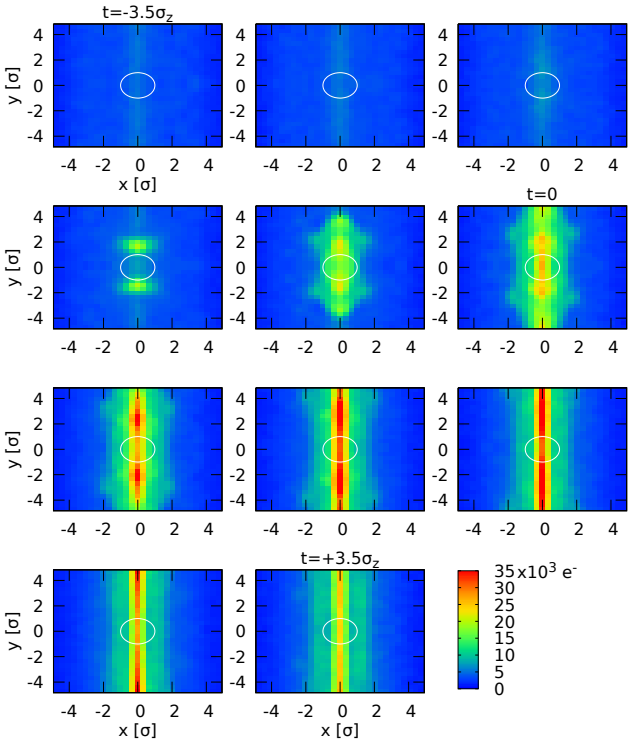

Figure 12: Transverse charge distributions of the electron cloud in an 800 Gauss dipole field during the passage of the last bunch of the 30 bunch train at 0.7 mA/b at 2.1 GeV, in the central region ($\pm 5\sigma$ of the beam size) for 11 time slices spanning $\pm 3.5\sigma_z$. One sigma of the beam size is shown as a white circle. Time increases from left to right, top to bottom. The time between slices is 20 ps.

small fraction (~0.1%) of photoelectrons are within the $\pm 5\sigma$ region around the beam, it is necessary to combine the results of many ECLOUD simulations to minimize statistical uncertainty in the calculation of the electric field.

The modeled tune shifts are calculated from the cloud space-charge electric field gradients. They can also be obtained from the tracking simulation described in the next section, and are found to be in agreement, but calculating them directly from the field gradients saves a step. The pinch effect, wherein the bunch attracts the nearby cloud as it passes, can be clearly seen in Figs. 14 and 15 as a dramatic increase in electric field gradients. However, since the bunch length is a mere 9 mm (16 mm) long at 2.1 mm (5.3 GeV), it hardly perturbs the built-up cloud during its passage. Additionally, for an offset bunch (the one being excited) in an on-axis train, the pinched cloud is found to be centered on the offset bunch, even in the presence of a dipole field (as shown in Fig. 16). Thus the kick on the offset bunch due to the pinched cloud can be neglected, and does not contribute to the coherent tune shift, as confirmed by the witness bunch betatron tune measurements shown in Fig. 17. The pinched cloud can however contribute to incoherent tune spread and emittance growth as demonstrated in the witness bunch measurements (Fig. 5). For this reason, the space-charge electric field gradients immediately prior to the bunch arrival are used when calculating the tune shifts.

SEY parameter determination

Tune shifts from simulation are found to depend strongly on a number of secondary electron yield parameters. Moreover, the effects of these parameters on the tune shifts can be highly correlated. Direct SEY measurements can provide a good starting point, but it is difficult to accurately measure all of the parameters. Furthermore, the ring-wide averaged SEY in the ring may be different than an external measurement of one piece of vacuum chamber. We use the model of secondary emission developed by Furman and Pivi and the SEY parameters determined for copper in [16] as a starting point. To improve agreement between the model and the various tune shift measurements, an optimizer is used to fit the SEY parameters to the tune shift measurements. At each iteration, the EC buildup simulations are run in parallel with the current best SEY parameters, and each parameter varied up and down by an adaptive increment. The tune shifts from these simulations are obtained, and the Jacobian is calculated and provided to the optimizer. The optimized input parameters are, in the notation of Furman and Pivi,

- $\hat{E}_{\mathrm{ts}}$: incident electron energy at which the true secondary yield is maximum for perpendicular incidence,
- s: true secondary SEY energy dependence parameter,

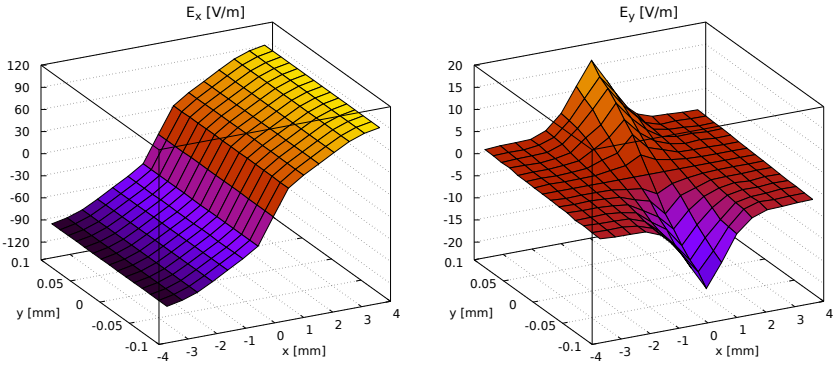

Figure 13: Space-charge electric field maps in a region of $\pm 5\sigma$ of the transverse beam size for the central time slice of the last bunch of the 30 bunch train at 0.7 mA/b at 2.1 GeV (see Fig. 12).

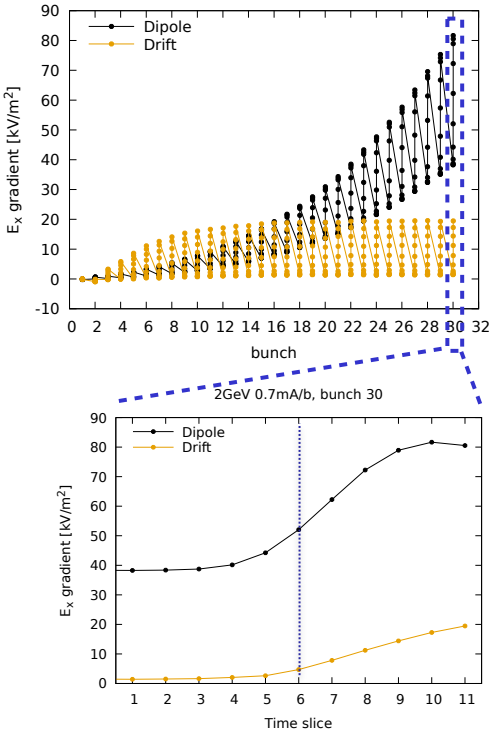

Figure 14: Top: horizontal electron cloud space-charge electric field gradients for the 11 time slices within each of 30 bunches, for dipoles and drifts. Bottom: electric field gradients for the 11 time slices in bunch 30, showing the center of the bunch at time slice 6.

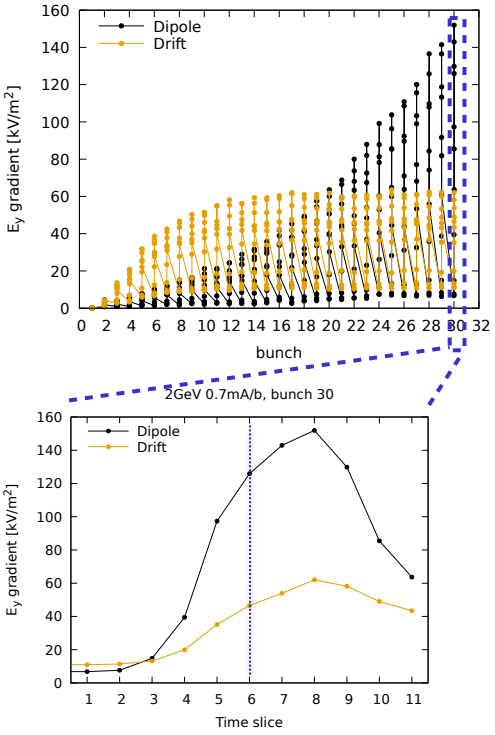

Figure 15: Top: vertical electron cloud space-charge electric field gradients for the 11 time slices within each of 30 bunches, for dipoles and drifts. Bottom: electric field gradients for the 11 time slices in bunch 30, showing the center of the bunch at time slice 6.

- $P_{\mathrm{l,r}}(\infty)$: rediffused secondary yield at high incident electron energy,
- $\hat{\delta}_{\mathrm{ts}}$: true secondary yield at perpendicular incidence,
- t_1 and t_2 : amplitude of the cosine dependence and power of the cosine in the true secondary yield: $\delta_{\mathrm{ts}}(\theta_{\mathrm{e}}) = \hat{\delta}_{\mathrm{ts}}[1 + t_1(1 - \cos^{t_2}\theta_{\mathrm{e}})]$, where $\theta_{\mathrm{e}} = 0$ for perpendicular electron incidence,
- t_3 and t_4 : amplitude of the cosine dependence and power of the cosine in true secondary peak energy: $E_{\mathrm{ts}}(\theta_{\mathrm{e}}) = \hat{E}_{\mathrm{ts}}[1 + t_3(1 - \cos^{t_4}\theta_{\mathrm{e}})]$,
- $\hat{P}_{\mathrm{l,e}}$: elastic yield in the low-energy limit, and
- ϵ and p : parameters for the energy distribution of the secondaries:

$$\frac{\mathrm{d}N}{\mathrm{d}E_{\mathrm{sec}}}(E_{\mathrm{sec}}) \propto \begin{cases} \dfrac{(E_{\mathrm{sec}}/\epsilon)^{p-1} e^{-E_{\mathrm{sec}}/\epsilon}}{\epsilon} & \text{for } E_{\mathrm{sec}} \leq 5\epsilon \\ 0 & \text{for } E_{\mathrm{sec}} > 5\epsilon \end{cases}.$$

Some of these parameters are highly correlated and could be removed from the optimization. The fits are performed simultaneously over all tune shift data at 2.1 and 5.3 GeV shown in Figs. 7 and 8.

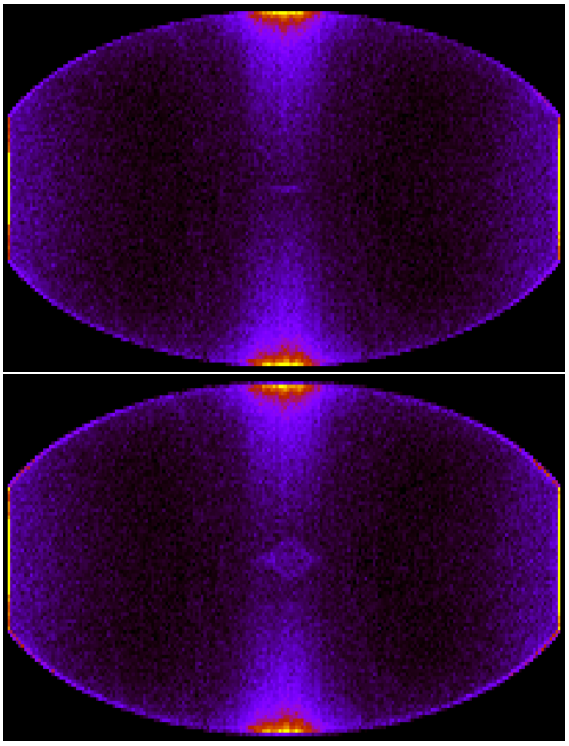

Figure 16: Simulated electron cloud density during the 3rd (top) and 6th (bottom) of 11 time slices during of the passage of bunch 15 (arbitrary), which has been offset from the centered bunch train by 1 mm horizontally to simulate the effect of kicking a single bunch when measuring its tune. The "pinched" cloud is found to be centered on the offset bunch position. The short bunch length (16 mm) bunch hardly modifies the larger built-up cloud. The simulated bunch current is 2 mA/b. At higher currents, the vertical band widens (4 mA/b) and splits into two (6 mA/b).

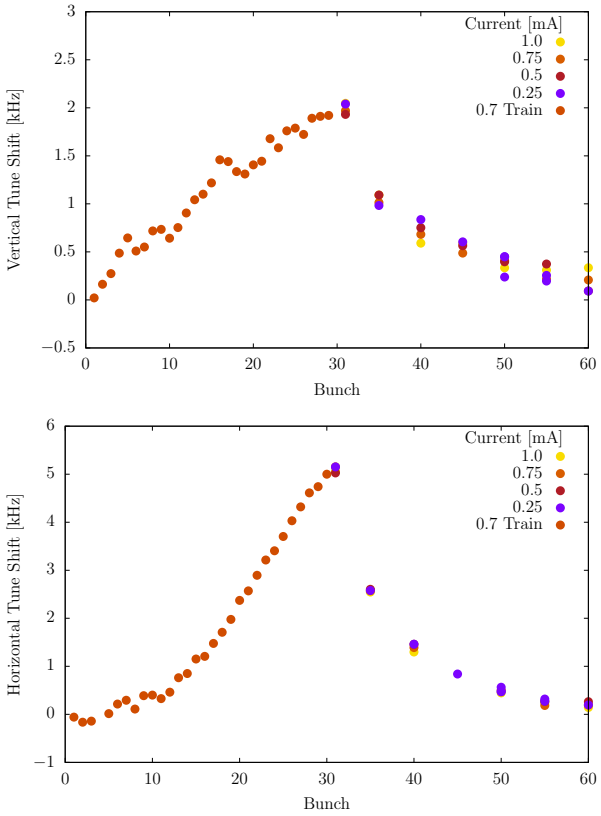

Figure 17: Vertical (top) and horizontal (bottom) tune shifts in kHz (to be compared to the revolution frequency of 390 kHz), measured using the digital tune tracker, for a 30 bunch train of positrons at 0.7 mA/b (1.12×10^{10} bunch population) at 2.1 GeV, followed by a witness bunch in bunch positions 31–60 at currents of 0.25, 0.5, 0.75, and 1.0 mA. The vertical tune shift from impedance (~1.0 kHz/mA) has been subtracted to show just the effects from EC. No dependence of the tune of the witness bunch on the witness bunch current is seen.

Beam particle tracking

The particle tracking simulations use a custom beam-cloud interaction element in Bmad overlaid on the dipole or drift elements and use the full CESR lattice. The electric fields from the different time slices are linearly interpolated to give the value of the fields at the x, y, and t of each particle. To include the effect of uncorrected vertical dispersion and its contribution to the vertical emittance, we give random Gaussian-distributed offset errors to the lattice so as to match the measured single-bunch vertical bunch size in simulation.

RESULTS

The comparison of tune shifts from simulation to measurements is shown in Figs. 18 and 19. After fine adjustment of the SEY parameters from the optimizer, excellent agreement is found over a range of bunch currents and energies.

Vertical bunch size growth in the tracking simulations over 100,000 turns is shown in Fig. 20. Equilibrium bunch size is calculated by averaging over the last 20,000 turns and is also shown in Fig. 20 with comparison to data. We see no bunch size growth in simulations or data for the 0.4 mA/b trains, but the growth is evident in both for the 0.7 mA/b positron train. Figure 21 shows the measurements for witness bunches for a 0.7 mA/b train where the witness bunch current is varied from 0.25 mA to 1.0 mA in 0.25 mA steps. We see that the witness bunch current has a strong effect on the bunch size, indicating a contribution by the pinch effect to the equilibrium emittance. This effect is also seen in the simulations.

SUMMARY

Vertical and horizontal emittance growth measurements along a train of positron bunches including a witness bunch were shown. Measurements of the vertical bunch size of the witness bunch varying its bunch population and distance from the train show emittance growth which scales both with shorter distances from the train (more cloud), and witness bunch current (more pinch effect).

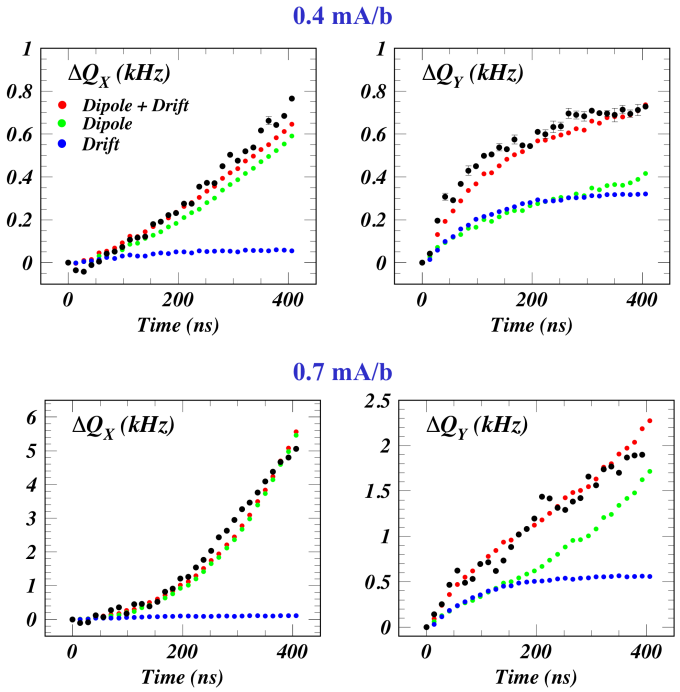

Figure 18: Horizontal (left) and vertical (right) tune shifts from data (black) and simulations (red: sum of dipoles (green) and drifts (blue)) for 30 bunch trains of positrons at 0.4 and 0.7 mA/b (0.64×10^{10} and 1.12×10^{10} bunch populations) at 2.1 GeV.

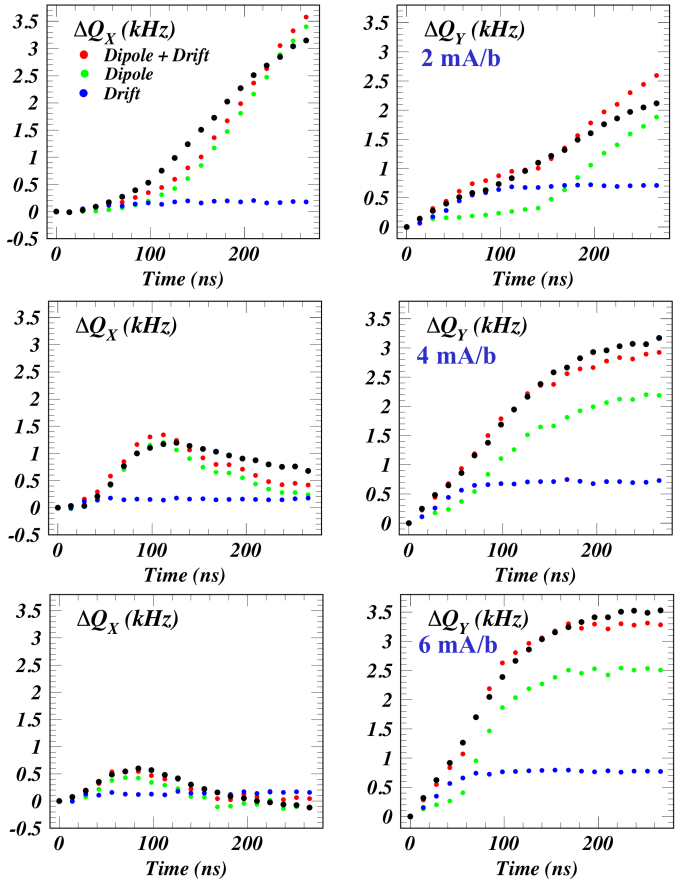

Figure 19: Horizontal (left) and vertical (right) tune shifts from data (black) and simulations (red: sum of dipoles (green) and drifts (blue)) for 20 bunch trains of positrons at 2, 4, and 6 mA/b ($3.2–9.6 \times 10^{10}$ bunch populations) at 5.3 GeV.

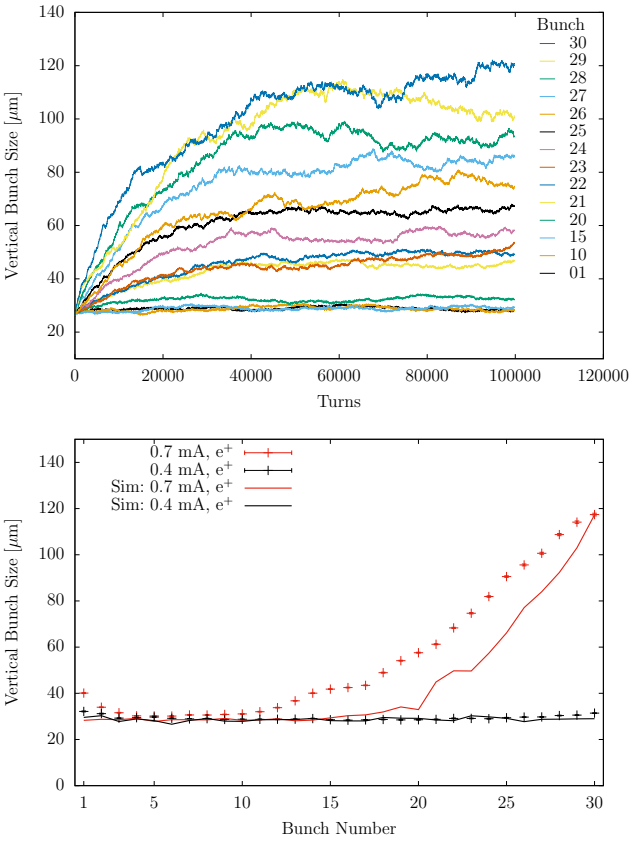

Figure 20: Top: vertical bunch size versus turn number from tracking simulations for 30 bunches of positrons at 0.7 mA/b (1.12×10^{10} bunch population) at 2.1 GeV. Bottom: Equilibrium vertical bunch size, obtained as the average of the last 20,000 turns, versus bunch number in simulations (lines) compared to measurements (points).

We have obtained improved measurements of betatron tune shifts along trains of positron bunches in the horizontal and vertical planes for a range of bunch populations, enabling advances in the predictive power of electron cloud buildup modeling. The Synrad3D and Geant4 simulation codes were employed to eliminate ad hoc assumptions in photoelectron production rates and kinematics characteristic of prior buildup simulations (see Ref. [8] for details). Electron cloud model parameters for secondary electron yield processes were determined through tune shift modeling optimized to the measurements. Excellent agreement in tune shifts were obtained over a range of beam currents and energies. The validated model was then used in a tracking simulation of the beam particles over many radiation damping times with electron cloud elements overlaid on the dipole and field-free regions. The simulations predict vertical emittance growth in agreement with the measurements. These results show that emittance growth due to electron cloud, modeled as an incoherent phenomenon is in good agreement with measurements when centroid bunch motion is damped with turn-by-turn feedback.

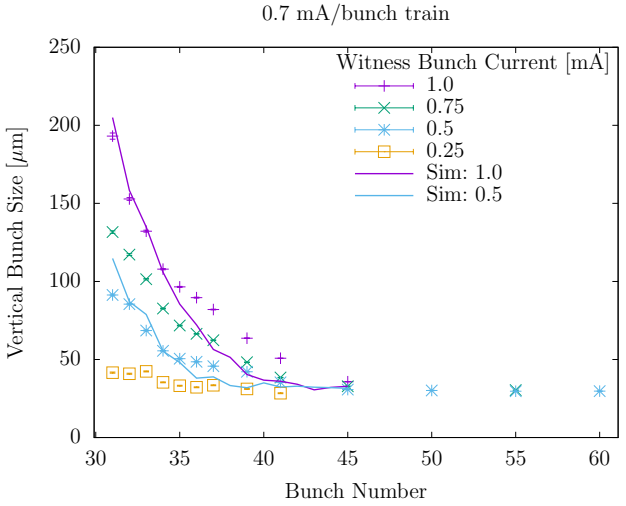

Figure 21: Vertical bunch size from tracking simulations (lines) compared to measurements (points) for witness bunches at various bunch currents following a 30 bunch train of positrons at 0.7 mA/b at 2.1 GeV.

ACKNOWLEDGMENTS

The authors wish to acknowledge important contributions from the technical staffs of the Wilson Laboratory. This work is supported by National Science Foundation and by the US Department of Energy under contract numbers PHY-0734867, PHY-1002467 and DE-FC02-08ER41538 and DE-SC0006505.

REFERENCES

[1] F. Zimmermann, "Electron-Cloud Effects in Past & Future Machines—Walk through 50 Years of Electron-Cloud Studies," in *Proceedings of ECLOUD 2012: Joint INFN-CERN-EuCARD-AccNet Workshop on Electron-Cloud Effects, La Biodola, Elba, Italy*, R. Cimino, G. Rumolo & F. Zimmermann, Eds., CERN, Geneva, Switzerland (2013), CERN-2013-002, p. 9–17.

[2] "The CESR Test Accelerator Electron Cloud Research Program: Phase I Report," Tech. Rep. CLNS-12-2084, LEPP, Cornell University, Ithaca, NY (Jan. 2013).

[3] S. Poprocki *et al.*, "Incoherent Vertical Emittance Growth from Electron Cloud at CesrTA," in *IPAC2016: Proceedings of the 7th International Particle Accelerator Conference, Busan, Korea* (2016), Paper TUPOR021.

[4] J. Crittenden *et al.*, "Electron Cloud Simulations for the Low-Emittance Upgrade at the Cornell Electron Storage Ring," in *NAPAC2016: Proceedings of the North American Particle Accelerator Conference, Chicago, IL* (2016), Paper TUPOB23.

[5] S. Poprocki *et al.*, "Incoherent Vertical Emittance Growth from Electron Cloud at CesrTA," in *NAPAC2016: Proceedings of the North American Particle Accelerator Conference, Chicago, IL* (2016), Paper WEA2CO03.

[6] G. Dugan & D. Sagan, "Simulating synchrotron radiation in accelerators including diffuse and specular reflections," *Phys. Rev. Accel. Beams* **20**, 020708 (Feb. 2017).

[7] S. Agostinelli *et al.*, "Geant4—a simulation toolkit," *Nuclear Instruments and Methods in Physics Research Section A: Accelerators, Spectrometers, Detectors and Associated Equipment* **506**, p. 250 – 303 (2003).

[8] J. Crittenden *et al.*, "Simulations of synchrotron-radiation-induced electron production in the CESR vacuum chamber wall," in *Proceedings of ECLOUD 2018: Joint INFN-CERN-EuroCirCol-ARIES-APEC Workshop on Electron-Cloud Effects, La Biodola, Elba, Italy*.

[9] J. P. Alexander *et al.*, "Vertical Beam Size Measurement in the CESR-TA e^+e^- Storage Ring Using X-Rays from Synchrotron Radiation," *Nucl. Instrum. Methods Phys. Res.* **A748**, p. 96–125 (Jun. 2014).

[10] S. Wang & R. Holtzapple, "Single-shot Bunch-by-Bunch Horizontal Beam Size Measurements using a Gated Camera at CesrTA," in *IPAC2016: Proceedings of the 7th International Particle Accelerator Conference, Busan, Korea* (2016), Paper MOPMR052.

[11] J. A. Crittenden *et al.*, "Progress in Studies of Electron-cloud-induced Optics Distortions at CesrTA," in *Proceedings of the 2010 International Particle Accelerator Conference, Kyoto, Japan*, ACFA (2010), p. 1976–1978.

[12] D. Sagan, "Bmad: A Relativistic Charged Particle Simulation Library," *Nucl. Instrum. Methods Phys. Res.* **A558**, p. 356–359 (Mar. 2006).

[13] B. L. Henke, E. M. Gullikson & J. C. Davis, "X-Ray Interactions: Photoabsorption, Scattering, Transmission, and Reflection at E = 50–30,000 eV, Z = 1–92," *At. Data Nucl. Data Tables* **54**, p. 181–342 (Jul. 1993).

[14] J. Allison *et al.*, "Recent developments in Geant4," *Nuclear Instruments and Methods in Physics Research Section A: Accelerators, Spectrometers, Detectors and Associated Equipment* **835**, p. 186 – 225 (2016).

[15] F. Zimmermann, G. Rumolo & K. Ohmi, "Electron Cloud Build Up in Machines with Short Bunches," in *ICFA Beam Dynamics Newsletter*, K. Ohmi & M. Furman, Eds., International Committee on Future Accelerators, No. 33, p. 14–24 (Apr. 2004).

[16] M. A. Furman & M. T. F. Pivi, "Probabilistic Model for the Simulation of Secondary Electron Emission," *Phys. Rev. ST Accel. Beams* **5**, 124404 (Dec. 2002).